RSC Advances

ROYAL SOCIETY OF CHEMISTRY

www.rsc.org/advances

Journal Name

COMMUNICATION

In vitro and in vivo applications of alginate/iron oxide nanocomposites for theranostic molecular imaging in brain tumor model

Received 00th January 20xx,
Accepted 00th January 20xx

DOI: 10.1039/x0xx00000x

www.rsc.org/

Chia-Hao Su[a] and Fong-Yu Cheng*[b]

Nanocomposites composed of highly biocompatible and safe alginate and iron oxide nanoparticles had been employed to encapsulate doxorubicine for brain tumor therapy. The antitumor activity of nanocomposites was demonstrated using *in vitro* and *in vivo* tests. The results significantly indicated nanocomposites had large safety and potential for brain tumor therapy.

Gliomas are the most aggressive and infiltrative brain tumor, but no therapeutic methods can efficiently cure it. The average survival time of a patient diagnosed with a glioma is less than 15 months.[1] Many anticancer drugs have been found to kill glioma cells *in vitro*, but their antitumor activities are largely limited in *in vivo* tests due to their poor solubility and short half-life in circulation. Combining targeted therapy with nanoparticle (NP)-based drug delivery can overcome these critical obstacles because of that Drug/NP complexs can prolong the circulation time in the blood and increase the local concentration of drugs in the tumor region.[2] However, the blood-brain barrier (BBB) provides a natural shield for the brain against the invasion of various toxins and restrict from passage only to necessary substrates from the circulation to the brain tissue.[3] Thus, the BBB also limits the brain uptake of diagnostic and therapeutic agents, which results in lower therapeutic efficiency.[4] Using BBB-disruption strategies to allow therapeutic agents to enter the brain is not suitable, because it may also allow circulating toxins in the blood to enter the brain.[3] Brain is more important than other tissues, so the used agents are highly required to be safe and cannot damage and affect brain functions. Therefore, an extensive and urgent search for real safe and effective platforms that can non-invasively deliver therapeutic drugs across the BBB to specifically kill glioma cells is under way.

Many studies of using NPs to increase drug delivery to the brain have been proved, and they showed different delivery efficiencies.[5] The base requirement of BBB-penetrating therapeutic agents is they must not damage the brain or cause adverse side effects. The ideal components of nanocomplexes must be biocompatible, biodegradable, and non-cytotoxic. Currently, most used carriers to cross the BBB are various functionalized liposomes.[6] However, the size control and stability of liposomes are problematic. Gold NPs are often used treating brain diseases because of their excellent biocompatibility and low cytotoxicity. Gold NPs decorated with peptides[7] or insulin[8] as BBB-penetrating platforms have also been reported. However, gold-based nanomaterials lack the detection ability in magnetic resonance imaging (MRI), a powerful modality for detecting the details of brain regions and diagnosing brain diseases. To mitigate this drawback, gadolinium (Gd^{3+}) chelates[7,9] or iron oxide NPs[10] are usually used to conjugated with gold-based nanomaterials to allow for MRI. In fact, the synthesized processes of functionalized gold nanocomplexes for MR applications are complicated and inconvenient. Thus, using magnetic nanomaterials as primary nanocarriers to directly allow MRI is better choice. For future clinical development, using materials that are already permitted by the U.S. Food and Drug Administration (FDA) to develop therapeutic agents is a better strategy due to they had completed clinical data and trials. However, the *in vivo* applications of nanomaterials composed of high safe or FDA-approved materials for brain tumors are still limited.

Here we report the development of a nanocarrier composed of alginate and Fe_3O_4 NPs and mainly focus on its safety and therapeutic efficiency. This nanocarrier can encapsulate an anticancer drug, doxorubicin (Dox), to treat brain tumor, both *in vitro* and *in vivo* (Scheme 1). Importantly, Fe_3O_4 NPs and alginate are highly safe, biocompatible and biodegradable materials, and they are permitted by the U.S. FDA for use in humans. Both materials had a wide variety of pharmaceutical, biomedical, biotechnology and tissue engineering applications. Moreover, the metabolites of Fe_3O_4 and alginate are also safe in human bodies and don't cause side effects.

The NH_2-exposed Fe_3O_4 NPs (NH_2-Fe_3O_4 NPs) were synthesized using the co-precipitation method previously described.[11] Subsequently, alginates were conjugated with NH_2-Fe_3O_4 NPs using

[a] Center for Translational Research in Biomedical Sciences, Kaohsiung Chang Gung Memorial Hospital, Kaohsiung 833, and Department of Biomedical Imaging and Radiological Sciences, National Yang Ming University, Taipei 112, Taiwan.
[b] Institute of Oral Medicine, National Cheng Kung University Hospital , College of Medicine, National Cheng Kung University, 1 University Road, Tainan City 701, Taiwan. E-mail: FYCheng@mail.ncku.edu.tw

† Electronic Supplementary Information (ESI) available: [Experimental details]. See DOI: 10.1039/x0xx00000x

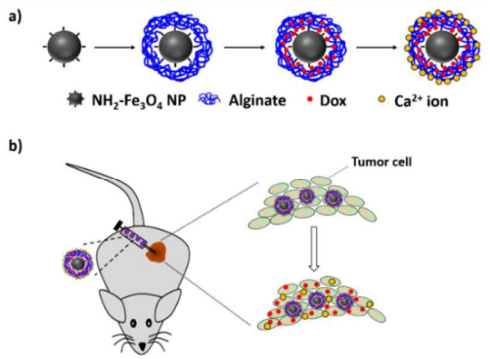

Scheme 1 (a) Schematic synthesis process of biosafe anticancer drug-encapsulating nanocarriers. b) Schematic mechanism of Dox-encapsulating nanocarriers and then Dox release from nanocarriers to brain tumor region to kill tumor cells.

a covalent bond on the particle surface. The true diameters of NH_2-Fe_3O_4 NPs and alginate-conjugated NH_2-Fe_3O_4 NPs (alg-Fe_3O_4 NPs) are separately calculated as 6.3 nm and 6.6 nm in transmission electron microscopy images (Fig. S1a). However, hydrodynamic diameter is preferred to be used in biomedical applications, so the hydrodynamic diameters of NH_2-Fe_3O_4 NPs and alg-Fe_3O_4 NPs were measured as 19.2 nm and 138.6 nm by dynamic light scattering (DLS) instrument (Fig. S1b). The discrepancy in hydrodynamic diameter of alg-Fe_3O_4 NPs is due to the existence of alginate on the surface of NPs, compared to NH_2-Fe_3O_4 NPs. The surface charge of the NH_2-Fe_3O_4 NPs was +20.3 mV. After conjugation with alginate, the surface charge of the alg-Fe_3O_4 NPs was -45.1 mV, which was contributed by COO^- groups of alginate. The change of surface charge and the discrepancy in hydrodynamic diameter of alg-Fe_3O_4 NPs indicated that alginate had been successfully tagged on the surface of NH_2-Fe_3O_4 NPs. The alginate on the Fe_3O_4 NP surface was also investigated using fourier transform infrared spectroscopy (FT-IR) (Fig. S2). The FT-IR spectrum of alg-Fe_3O_4 NPs involves both characteristic adsorption peaks of Fe_3O_4 NPs and alginate. The alginate content in the alg-Fe_3O_4 NPs was then determined by thermogravimetric analysis (TGA). A weight loss of about 12.1% was observed for the alg-Fe_3O_4 NPs (Fig. S3a), corresponding to the conjugated amount of approximately ~0.15 mg alginate per mg of Fe_3O_4 NPs.

To fabricate the Dox-encapsulated alg-Fe_3O_4 (Dox/alg-Fe_3O_4) NPs, Dox and alg-Fe_3O_4 NPs were mixed, and then 1 mM of calcium ion (Ca^{2+}) aqueous solutions were added to the mixture. When mixing Dox and alg-Fe_3O_4 NPs, alg-Fe_3O_4 NPs spontaneously captured Dox by electrostatic force due to the positive charges of DOX and the negative charges of alg-Fe_3O_4 NPs. The surface alginate of alg-Fe_3O_4 NPs was physically crosslinked by Ca^{2+} to form net structures, and then Dox was trapped inside the NPs. The morphology of Dox/alg-Fe_3O_4 NPs was shown in Fig. S1a. The saturated encapsulated amounts of Dox in Dox/alg-Fe_3O_4 NPs were ~1.42 mg Dox per mg of Fe_3O_4 NPs (Fig. S3b). To evaluate the Dox-trapped efficiencies of Dox/alg-Fe_3O_4 NPs, the Dox leaching of Dox/alg-Fe_3O_4 NPs were tested in deionized water and phosphate buffered saline (PBS) (10 mM, pH

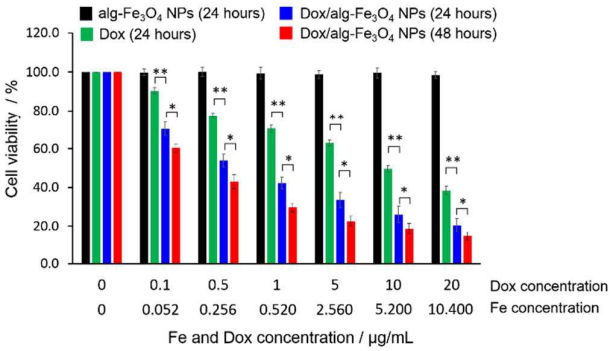

7.4) at 37 ℃ (Fig. S4a). The leaching percentages of Dox in both conditions in

Figure 1. *In vitro* cell viability of C6 cells incubated with free Dox, alg-Fe_3O_4 NP, and Dox/alg-Fe_3O_4 NPs at 37°C for 24 and 48 h. All experiments were repeated in triplicate. Asterisks indicate statistically significant different of both experimental sets. (*, P<0.1; **, P<0.01).

Fig. S4a are below 10% after 240 h. These results indicate that Dox efficiently trapped in the Dox/alg-Fe_3O_4 NPs. Fig. S4b shows the Dox release profiles of Dox/alg-Fe_3O_4 NPs in PBS (pH 5.5) and cytoplasm mimicking (CM) buffer at 37℃. The Dox-release rate of Dox/alg-Fe_3O_4 NPs in CM buffer was faster than in PBS (pH 5.5) because of the ethylenediamine tetraacetic acid (EDTA) in the CM buffer. EDTA can strongly grab the Ca^{2+} chelated with the alginate of the Dox/alg-Fe_3O_4 NPs and destroy the crosslink structures.

To determine what were safe doses of Dox/alg-Fe_3O_4 NPs for cell and animal experiments, Human umbilical vein endothelial cells (HUVECs) were incubated with different iron doses alg-Fe_3O_4 NPs at 37℃ for 24 and 48 h. The alg-Fe_3O_4 NPs showed no apparent cytotoxicity and the HUVECs had viability rates > 95% (Fig. S5). Subsequently, after 24 h of incubation with alg-Fe_3O_4 NPs, the cell viability of C6 brain cancer cells was > 95% (Fig. 1). To evaluate the efficacy of Dox/alg-Fe_3O_4 NPs in cancer cells, C6 cells were separately treated with Dox and Dox/alg-Fe_3O_4 NPs for 24 h. Cell viability was significantly lower in Dox/alg-Fe_3O_4 NP-treated C6 cells than in free-Dox-treated C6 cells at all Dox concentrations because the nanocarriers increased the amount of drugs delivered to the cells and then increased the drug dose inside the cells. After 48 h of treatment with Dox/alg-Fe_3O_4 NPs, cell viability was even lower according to statistical analysis ($p < 0.1$). Detail safety of alg-Fe_3O_4

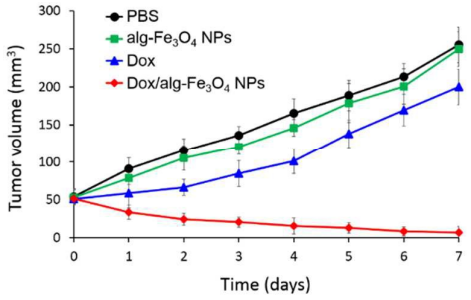

Figure 2. In vivo anti-tumor activity of Dox/alg-Fe3O4 NPs. The tumor volume of mice in all groups were measured every day. The mice were intratumorally injected with PBS (10 mM, pH 7.4), alg-Fe_3O_4 NPs, Dox only, or Dox/alg-Fe_3O_4 NPs. The injected Dox dose

was 3 mg/Kg of body weight, and the equivalently injected Fe dose was 5 mg/Kg of body weight. (n=5)

NPs was evaluated by determining the activities of liver enzymes (glutamate oxaloacetate transaminase [GOT], glutamic-pyruvic transaminase [GPT], total bilirubin [T-Bil), and alkaline phosphatase [ALP]) and kidney enzymes (blood urea nitrogen [BUN], creatinine [CREA], and uric acid [UA]) of mice with treatment with alg-Fe_3O_4 NPs (Fig. S6). The levels of GOT, GPT, tT-Bil, and ALP of alg-Fe_3O_4 NP-treated mice have no obvious difference compared to those of PBS-treated mice (control group) (Fig. S6a). No apparent changes were also obtained in the levels of BUN, T-Bil, and UA of alg-Fe_3O_4 NP-treated mice (Fig. S6b). It represents no cytotoxic effects are toward the liver and kidney functions of alg-Fe_3O_4 NPs-treated mice. Similarly, the histological studies of alg-Fe_3O_4 NP-treated mice also had no change (Fig.S7) and indicated alg-Fe_3O_4 NPs were safe for use in clinical applications.

The efficacy of Dox/alg-Fe_3O_4 NPs was next evaluated in an *in vivo* animal model by measuring tumor growth and body weight in mice with C6 tumors (~50 mm^3), which were divided int o four treatment cohorts (PBS, free Dox, alg-Fe_3O_4 NPs, and Dox/alg-Fe_3O_4 NPs) (Fig. 2). All the mice were intratumorally injected with one of the four treatments. The Dox dose for each Dox-treated mouse was 3 mg/Kg. The equivalent Fe dosage of Dox/alg-Fe_3O_4 NPs was 5 mg/Kg when the injection dose of Dox was 3 mg/Kg. Thus, the injection doses of the control groups (free Dox and alg-Fe_3O_4 NPs) were 3 mg/Kg of Dox and 5 mg/Kg of Fe, respectively. The growth of C6 tumors was not inhibited in the PBS, alg-Fe_3O_4 NPs, or free Dox groups compared with the Dox/alg-Fe_3O_4 NPs group (Fig. 2). However, tumor growth was significantly inhibited in Dox/alg-Fe_3O_4 NPs group. The primary reason for this outcome is that C6 cells can uptake Dox/alg-Fe_3O_4 NPs, and then most of their Dox is released in the cytoplasm and then enters the cell nuclei to cause cell apoptosis. Conversely, C6 cells prevented free Dox from entering. There were no significant differences in mean body weights of the four groups of mice (Fig. S8), which showed none of the treatments caused negative side effects. To investigate the possible therapeutic effects of future clinical applications using Dox/alg-Fe_3O_4 NPs for *in vivo* human brain cancer,

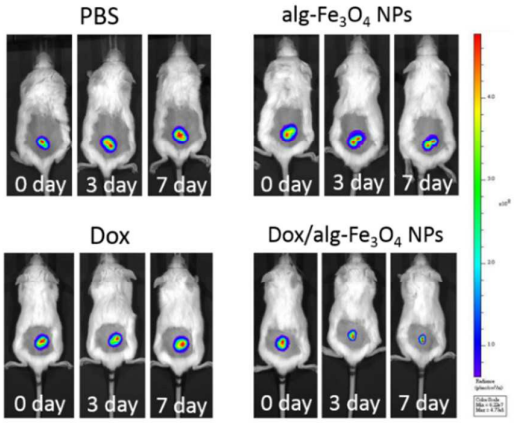

Figure 3. In vivo anti-tumor activity of Dox/alg-Fe_3O_4 NPs in mice with U87MG-luc2 tumors ~50 mm3 during the experimental period. All images are luminescence images from U87MG-luc2 cells and monitored using the IVIS imaging system. The mice were intratumorally injected with PBS (10 mM, pH 7.4), alg-Fe_3O_4 NPs, Dox only, and Dox/alg-Fe_3O_4 NPs. The injected Dox dose was 3 mg/Kg of body weight and the equivalently injected Fe dosage was 5 mg/Kg of body weight. (n=5)

the U87MG-luc2 human glioblastoma cell line, which expresses luciferase, was selected to establish our animal model of U87MG-luc2 tumor-bearing mice, which were divided into four treatment-based cohorts: PBS, Dox, alg-Fe_3O_4 NPs, and Dox/alg-Fe_3O_4 NPs. The alg-Fe_3O_4 NPs, Dox/alg-Fe_3O_4 NPs, free Dox, and Dox/alg-Fe_3O_4 NPs were intratumorally injected into the tumor site, and then the tumor size was monitored pre-injection and at 3 and 7 days post-injection using the IVIS image system. Tumors continuously grew in PBS-treated mice. In the mice treated with Dox and alg-Fe_3O_4 NPs, the tumor sizes showed no obvious variations until 7 days post-injection. Comparatively, tumors significantly shrank by about 50% in the mice treated with Dox/alg-Fe_3O_4 NPs. It seems that releasing the Dox directly inside mice, most of the Dox remained outside the tumor cells and had no anti-tumor effect. In order to achieve the objective of anti-tumor therapy, the mice with smaller tumors (~25 mm^3) were injected with Dox/alg-Fe_3O_4 NPs under the same experimental conditions and procedures as shown in Fig. 3. The U87MG-luc2 tumors hadalmost disappeared on post-injection day 3 (Figure S9). On post-injection day 7, the tumor had totally disappeared from the backs of some mice. This indicates that tumors smaller than 25 mm^3 can be completely remitted after treatment with Dox/alg-Fe_3O_4 NPs with a Dox dose of 3 mg/Kg. Thus, we hypothesize that the Dox/alg-Fe_3O_4 NPs can be used for brain tumor therapy in future clinical trials.

In summary, a novel nanocomposite composed of highly safe and US-FDA-approved Fe_3O_4 NPs and alginate has been synthesized and they could encapsulate Dox inside the particles. The Dox leaching percentage of Dox/alg-Fe_3O_4 NPs is quite low in deionized water and PBS, but Dox can be released from Dox/alg-Fe_3O_4 NPs inside the tumor cells after cellular uptake. Both *in vitro* and *in vivo* experimental results showed that the Dox/alg-Fe_3O_4 NPs inhibited C6 tumor cell growth and killed them without damaging healthy non-tumor cells. Moreover, U87MG-luc2 tumor-bearing mice with larger and smaller tumors (~50 mm^3 and ~25 mm^3) are being designed to test the anti-tumor activity of Dox/alg-Fe_3O_4 NPs. Based on our results in this study, we are designing and proceeding with additional animal experiments for primary brain tumor therapy by inducing U87MG-luc2 tumor in mice brain to establish glioblastoma models. The BBB-permeating NPs based on Dox/alg-Fe_3O_4 NPs are expected to develop. The BBB-permeating NPs will be intravenously injected into mice with U87MG-luc2 tumors to demonstrate that these BBB-permeating NPs will cross the BBB and provide efficacious anti-brain-tumor therapy.

Notes and references

1 J. T. Huse, E. C. Holland, *Nat. Rev. Cancer* 2010, **10**, 319-331.
2 I. van Rooy, S. Cakir-Tascioglu, W. E. Hennink, G. Storm, R. M. Schiffelers, E. Mastrobattista, *Pharm. Res.* 2011, **28**, 456-471.
3 X. Gao, C. Li, *Small* 2014, **10**, 426-440.

4 (a) R. Cecchelli, V. Berezowski, S. Lundquist, M. Cilot, M. Renftel, M. P. Dehouck, L. Fenart, *Nat. Rev. Drug Discovery* 2007, **6**, 650-661.
5 (a) R. M. Koffie, C. T. Farrar, L. –J. Saidi, C. M. William, B. T. Hyman, *PNAS.* 2011, **108**, 18837-18842; (b) D. Ni, J. Zhang, W. Bu, H. Xing, F. Han, Q. Xiao, Z. Yao, F. Chen, Q. He, J. Liu, S. Zhang, W. Fan, L. Zhou, W. Peng, J. Shi, *ACS Nano* 2014, **8**, 1231-1242.
6 (a) K. Ulbrich, T. Knobloch, J. Kreuter, *J. Drug Targeting* 2011, **19**, 125-132; (b) J. Q. Gao, Q. Lv, L. M. Li, X. J. Tang, F. Z. Li, Y. L. Hu, M. Han, *Biomaterials* 2013, **34**, 5628-5639.
7 Y. Cheng, Q. Dai, R. A. Morshed, X. Fan, M. L. Wegscheid, D. A. Wainwright, Y. Hau, L. Zhang, B. Auffinger, A. L. Tobias, E. Rincon, B. Thaci, A. U. Ahmed, P. C. Warnke, C. He, M. S. Lesniak, *Small* 2014, **10**, 5137-5150.
8 M. Shilo, M. Motiei, P. Hana, R. Popovtzer, *Nanoscale* 2014, **6**, 2146-2152.
9 M. F. Kircher, A. de la Zerda, J. V. Jokerst, C. L. Zavaleta, P. J. Kempen, E. Mittra, K. Pitter, R. Huang, C. Campos, F. Habte, R. Sinclair, C. W. Brennan, I. K. Mellinghoff, E. C. Holland, S. S. Gambhir, *Nat. Med.* 2012, **18**, 829-834.
10 L. Li, M. Nurunnabi, Y. Y. Jeong, Y. Lee, K. M. Huh, *J. Mater. Chem. B* 2014, **2**, 2929-2937.
11 D. B. Shieh, F. Y. Cheng, C. H. Su, C. S. Yeh, M. T. Wu, C. Y. Tsai, C. L. Wu, D. H. C, C. H. Chou, *Biomaterials* 2005, *26*, 7183-7191.
12 M. Sivasubramanian, Y. Hsia, L. W. Lo, *Frontiers in Molecular Biosciences* 2014, **1**, 1-16.